



HHS Public Access

Author manuscript

Adv Mater. Author manuscript; available in PMC 2019 February 01.

Published in final edited form as:

Adv Mater. 2018 February ; 30(7): . doi:10.1002/adma.201705383.

Activatable Protein Nanoparticles for Targeted Delivery of Therapeutic Peptides

Dr. Xi Yu,

Department of Neurosurgery, Yale University, New Haven, CT 06511, USA

Prof. Xingchun Gou,

Department of Neurosurgery, Yale University, New Haven, CT 06511, USA

Shaanxi Key Laboratory of Brain Disorders & Institute of Basic and Translational Medicine, Xi'an Medical University, Xi'an 710021, China

Prof. Peng Wu,

Department of Neurosurgery, Yale University, New Haven, CT 06511, USA

Department of Neurosurgery, Renmin Hospital of Wuhan University, Wuhan, Hubei 430060, China

Dr. Liang Han,

Department of Neurosurgery, Yale University, New Haven, CT 06511, USA

Dr. Daofeng Tian,

Department of Neurosurgery, Yale University, New Haven, CT 06511, USA

Dr. Fengyi Du,

Department of Neurosurgery, Yale University, New Haven, CT 06511, USA

Dr. Zeming Chen,

Department of Neurosurgery, Yale University, New Haven, CT 06511, USA

Dr. Fuyao Liu,

Department of Neurosurgery, Yale University, New Haven, CT 06511, USA

Dr. Gang Deng,

Department of Neurosurgery, Yale University, New Haven, CT 06511, USA

Ann T. Chen,

Department of Neurosurgery, Yale University, New Haven, CT 06511, USA

Prof. Chao Ma,

Department of Neurosurgery, Yale University, New Haven, CT 06511, USA

Correspondence to: Jiangbing Zhou.

The ORCID identification number(s) for the author(s) of this article can be found under <https://doi.org/10.1002/adma.201705383>.

Supporting Information

Supporting Information is available from the Wiley Online Library or from the author.

Conflict of Interest

The authors declare no conflict of interest.

Dr. Jun Liu,

Department of Neurosurgery, Yale University, New Haven, CT 06511, USA

Dr. Sara M. Hashmi,

Department of Chemical and Environmental Engineering, Yale University, New Haven, CT 06511, USA

Dr. Xing Guo,

Department of Neurosurgery, Yale University, New Haven, CT 06511, USA

Prof. Xiaolong Wang,

Shaanxi Key Laboratory of Brain Disorders & Institute of Basic and Translational Medicine, Xi'an Medical University, Xi'an 710021, China

Prof. Haitian Zhao,

Department of Neurosurgery, Yale University, New Haven, CT 06511, USA

Dr. Xinran Liu,

Department of Cell Biology, Yale University School of Medicine, New Haven, CT 06510, USA

Prof. Xudong Zhu,

Institute of Biochemistry and Molecular Biology, College of Life Sciences, Beijing Normal University, Beijing 100875, China

Prof. Kevin Sheth,

Department of Neurology, Yale University, New Haven, CT 06510, USA

Prof. Qianxue Chen,

Department of Neurosurgery, Renmin Hospital of Wuhan University, Wuhan, Hubei 430060, China

Prof. Louzhen Fan, and

Department of Chemistry, Beijing Normal University, Beijing 100875, China

Prof. Jiangbing Zhou

Department of Neurosurgery, Yale University, New Haven, CT 06511, USA

Abstract

Clinical translation of therapeutic peptides, particularly those that require penetration of the cell membrane or are cytolytic, is a major challenge. A novel approach based on a complementary mechanism, which has been widely used for guided synthesis of DNA or RNA nanoparticles, for de novo design of activatable protein nanoparticles (APNPs) for targeted delivery of therapeutic peptides is described. APNPs are formed through self-assembly of three independent polypeptides based on pairwise coiled-coil dimerization. They are capable of long circulation in the blood and can be engineered to target diseases. Peptides to be delivered are incorporated into APNPs and released into the disease microenvironment by locally enriched proteases. It is demonstrated that APNPs mediate efficient delivery of NR2B9c, a neuroprotective peptide that functions after cell penetration, and melittin, a cytolytic peptide that perturbs the lipid bilayer, for effective treatment of stroke and cancer, respectively. Due to their robust properties, simple design, and economic

costs, APNPs have great potential to serve as a versatile platform for controlled delivery of therapeutic peptides.

Keywords

breast cancer; nanoparticles; peptides; stroke; targeted delivery

Therapeutic peptides have emerged as one of the most important classes of new pharmaceuticals. A recent survey revealed that 11% of drugs approved by the FDA from 2009 to 2011 are peptides.^[1] In total, there are about 100 peptides that have received approval for clinical use in the United States and other countries.^[1,2] In addition, \approx 200 peptides are being tested in clinical trials and at least 400 peptides are being studied in advanced preclinical stages.^[1,2]

Therapeutic peptides can be classified into three different types, based on their biological properties and functional mechanisms. Type I peptides have limited toxicity and exert their pharmacological function without penetrating the cell membrane. The Nogo extracellular peptide 1–40 (NEP 1–40) is a type I 40-amino acid peptide that has axonal regeneration and functional recovery capabilities.^[3] Type II peptides are also nontoxic but function intracellularly and thus require penetration of the cell membrane. NR2B9c is a promising type II neuroprotective peptide for patients with acute stroke.^[4,5] Type III peptides are cytolytic and cannot be directly administered systemically at a therapeutically effective dose. Melittin is a potent type III anticancer peptide.^[6]

Compared to small molecule drugs, therapeutic peptides typically have higher levels of biological activity and specificity.^[1,2] Due to poor oral bioavailability, therapeutic peptides are often administered intravenously in clinic. However, clinical translation of therapeutic peptides has been limited by their chemical nature. Peptides are natural targets to over 600 types of proteases in the human body. In addition, most peptides are rapidly recognized by the reticuloendothelial system (RES) and cleared out by macrophages. Consequently, therapeutic peptides often have a short half-life in the circulatory system. Translation of type II and type III peptides is particularly challenging. Type II peptides, which interact with intracellular targets, require conjugation of cell penetrating peptides (CPPs) to achieve cell penetration. As most CPPs cross cell membrane without selectivity, conjugation of CPPs to type II peptides leads to nonspecific binding to cells in the circulatory system, leading to further reduction of half-life and increase of off-target effects.^[7] On the other hand, type III peptides are highly toxic. Translation of peptides in this group has been unsuccessful.

To facilitate translation of therapeutic peptides, we designed activatable protein nanoparticles (APNPs), in which therapeutic peptides are embedded in APNP backbone and thus do not exhibit activities in the circulatory system. After intravenous administration, APNPs home to the target tissue, where they are activated by proteases enriched in the disease microenvironment. As a result, active peptides are released within the disease location. Specifically, we constructed APNPs through self-assembly of three independent polypeptides based on pair-wise interaction, an assembly mechanism that is often used to guide the synthesis of DNA or RNA nanoparticles.^[8] An individual polypeptide consists of

one or more therapeutic peptides flanked by two coiled-coil forming motifs jointed with a “self” peptide (Figure 1a,b). Enzyme-responsive sequences are located between therapeutic peptides and the coiled-coil motifs. Modular peptide fragments are connected using a peptide linker with the sequence SGPG to provide hinge flexibility at the vertices. The “self” peptide is employed to enhance the circulation of nanoparticles through inhibition of macrophage-mediated clearance by the RES.^[9] A 2000 Da polyethylene glycol (PEG) molecule conjugates to a cysteine residue within the polypeptide to prevent aggregation and improve the nanoparticle’s solubility and blood circulation. Heterodimeric coiled-coil pairs are employed to promote tethering among polypeptides through dimerization.^[10] Because of the high specificity of pairwise coiled-coil dimerization, three polypeptides mixed at equal mole are self-assembled into protein nanoparticles. After reaching the disease microenvironment, the locally enriched proteases cleave the enzyme-responsive sequences and release active peptides (Figure 1c). Modular peptides and their sequences are illustrated in Figure 1a.

We evaluated APNPs for systemic delivery of Tat-NR2B9c, a type II peptide. *N*-Methyl-D-aspartate receptor (NMDAR)-dependent excitotoxicity, which is induced by the binding of postsynaptic density protein-95 (PSD-95) with NMDARs and neuronal nitric oxide synthase (nNOS) at excitatory synapses, is the primary mechanism of neuronal injury following stroke.^[4,11] A promising approach to protecting neurons against NMDAR-mediated excitotoxicity is to disrupt the interaction of NMDARs with PSD-95, which can be achieved using the last nine amino acids of the carboxyl tail of GluN2B (NR2B9c).^[4] NR2B9c cannot penetrate cell membrane by itself. Therapeutic use of NR2B9c requires fusion with the TAT peptide, a CPP derived from TAT protein in the human immunodeficiency virus.^[4] The resulting Tat-NR2B9c peptide has been shown to reduce the infarct volume in rats and nonhuman primates post ischemic insult after intravenous administration.^[4,12] Tat-NR2B9c was evaluated in human patients with iatrogenic stroke in the Evaluating Neuroprotection in Aneurysm Coiling Therapy (ENACT) trial. Although treatment with Tat-NR2B9c reduced the number of lesions in the brain, no difference in the volume of lesions was found between the treatment and placebo groups.^[5] The failure of the ENACT trial may not be a surprise. In addition to poor stability and short half-life that are characteristics of most peptides, TAT-based therapeutics is further hindered by the lack of tissue specificity. TAT-based CPP penetrates most biological membranes without selectivity and thus nonspecifically binds to cells or organs during circulation.^[7] It is possible that intravenous administration of Tat-NR2B9c in human patients does not allow the delivery of a pharmacologically significant amount of peptide to the brain.

To enhance the delivery of Tat-NR2B9c, we incorporated Tat-NR2B9c into APNPs. Tat-NR2B9c is flanked by TPRSFL, a peptide that is sensitive to enzymatic cleavage by thrombin.^[13] Individual polypeptides containing Tat-NR2B9c were expressed in *Escherichia coli* and purified (Figure 2a). Isothermal titration calorimetry (ITC) analysis confirmed that the polypeptides interact with each other with binding affinity (K_D) values ranging from 13×10^{-6} to 55×10^{-6} M (Figure S1, Supporting Information). The endothermic binding enthalpies for those interactions are high ($H = 8\text{--}20$ kcal mol⁻¹) with favorable G values of -3 to -7 kcal mol⁻¹. Three polypeptides in combination formed APNPs (Figure 2b). Transmission electron microscopy (TEM) revealed that the resulting Tat-NR2B9c-loaded

APNPs, designated as TN-APNPs, were spherical in morphology and 7.1 nm in diameter (Figure 2c), which was also visualized by atomic force microscopy (AFM; Figure S2a, Supporting Information). Conjugation of PEG was beneficial for improving the solubility of APNPs, although it did not affect APNP formation (Figure S2b, Supporting Information). Compared to APNPs synthesized using polypeptides without “self” motif (Figure S2c, Supporting Information), APNPs bearing “self” motif demonstrated a prolonged circulation time in the blood (Figure S2e, Supporting Information). Inclusion of the “self” motif did not change the size of APNPs (Figure S2d, Supporting Information). Due to the existence of TPRSFL, TN-APNPs disassembled in response to thrombin treatment (Figure 2d). APNPs could be synthesized with high reproducibility (Figure S2f, Supporting Information).

There are five lines of evidence supporting that TN-APNPs were assembled as designed. First, we found that three polypeptides in combination, but not individual ones, formed APNPs (Figure 2b). Second, we incubated TN-APNPs (without removal of His tags from polypeptides) with 5 nm Ni-NTA–nanogold beads. After extensive washing, TN-APNPs were subjected to TEM. Results in Figure 2c showed that three Ni-NTA–nanogold beads were incorporated into APNPs (Figure 2c). Although the reason why incorporation of nanogold beads increased the size of APNPs is to be further investigated, this finding suggests that TN-APNPs were formed through assembly of three polypeptides. Third, circular dichroism (CD) spectroscopy revealed a highly organized, helical secondary structure in TN-APNPs, suggesting that the formation of TN-APNPs was driven by coiled-coil dimerization (Figure 2e). In contrast, similar structures were not identified in any individual polypeptides (Figure S2g, Supporting Information). Fourth, multiangle static light scattering (MALS) analysis of single polypeptide (monomer PP3), two-polypeptide assembly (dimer, PP2 + PP3), and three-polypeptide assembly (trimer, TN-APNPs) found that only the three-polypeptide assembly exhibits isotropic scattering and power law dependence of I on q , suggesting that TN-APNP is a globular aggregate of three polypeptides (Figure S2h, Supporting Information). Fifth, analytical ultracentrifugation (AUC) analysis of the same set of samples found that the sediment coefficients ($S_{20,w}$) for monomer, dimer, and trimer exhibited gradual increase, with 2.2 s for monomer, 3.2 s for dimer, and 4.6 s for trimer (Figure S2i, Supporting Information), which correlate with molecular weights of ≈ 22.1 , ≈ 43.6 , and ≈ 63.6 kDa. The molecular weights estimated by AUC well match the molecular weights of monomer, dimer, and trimer predicted by the design, which are 21.6, 41.1, and 63.2, respectively.

APNPs significantly improved the delivery of Tat-NR2B9c to the ischemic brain. We labeled both free Tat-NR2B9c peptides and TN-APNPs with AF750, a near-infrared fluorescent dye that allows for noninvasive detection using an IVIS imaging system, and evaluated their stroke target effect in rats that received 90 min middle cerebral artery occlusion (MCAO). 24 h after intravenous administration, the brains were harvested and imaged. Based on the fluorescence intensity, the concentration of Tat-NR2B9c accumulated in the ischemic region was 5.1-fold greater in rats that received treatment of APNPs than in rats that received treatment of free peptide (Figure 2f; Figure S3a, Supporting Information). In addition to high efficiency, APNPs also demonstrated great specificity for the ischemic region. We sectioned the brains isolated from rats that received treatment of AF750-labeled TN-APNPs. The brain slices were further subjected to 2,3,5-triphenyltetrazolium chloride (TTC) staining

and IVIS imaging. Our results suggest that the location of ischemic tissue (white, TTC staining signal) overlapped with the location of nanoparticles (red to yellow, AF750 signal; Figure S3c, Supporting Information). Fluorescence was also found in the penumbra region surrounding the ischemic core. In contrast, images of the brains isolated from rats that received treatment of free Tat-NR2B9c did not result in the same degree of specificity in the ischemic regions (Figure S3b, Supporting Information).

We assessed the efficacy of intravenous administration of TN-APNPs in rats with MCAO. Control rats received treatment with either free peptide at equal mole or phosphate-buffered saline (PBS). Treatments were performed at 0, 24, and 48 h after surgery. The dose of TN-APNPs was 22 μ g per rat. An equivalent mole of Tat-NR2B9c was used in the free peptide group. 24 h after the last treatment, rats were euthanized and the brains were harvested and subjected to standard TTC staining. We found that treatment of TN-APNPs significantly reduced the infarct sizes. The average percentage of infarct sizes in the TN-APNP treatment group was 22.6%, compared to 58.8% and 38.7% for rats treated with PBS and free Tat-NR2B9c, respectively (Figure 2g; Figure S3d, Supporting Information). Consistent with the reduction of infarct size, we found that TN-APNP treatment significantly improved neurological performance. On the postoperative day, 8 out of 11 (73%) rats receiving treatment of TN-APNPs did not display obvious neurological deficits, whereas only 1 out of 11 (9%) of rats receiving PBS or the same dose of free peptide showed comparable neurological function (Figure 2h).

Confocal microscopy revealed that Tat-NR2B9c colocalized with PSD-95 within cells, suggesting that Tat-NR2B9c was released from TN-APNPs through thrombin cleavage after reaching the ischemic microenvironment and subsequently penetrated cells, presumably through the interaction of Tat with cell membrane. The colocalization of Tat-NR2B9c with PSD-95 only occurred ipsilateral to the hemisphere of MCAO surgery, which is consistent with the infarcted area, suggesting that the observed biological effect of TN-APNPs was due to the release of free Tat-NR2B9c (Figure 2i). In contrast, the colocalization of Tat-NR2B9c with PSD-95 was not seen in the contralateral nonischemic hemisphere (Figure S4, Supporting Information).

Next, we evaluated APNPs for systemic delivery of melittin, a type III peptide. Melittin, a cytolytic peptide derived from the venom of the honeybee *Apis mellifera*, is a promising anticancer agent.^[6] However, as a type III peptide, melittin attacks lipid membranes without specificity and thus induces significant toxicity after intravenous administration, which impedes its clinical applications.^[6,14] We evaluated APNPs for melittin delivery by replacing Tat-NR2B9c and TPRSFL in the TN-APNPs with melittin and PLGLAG, respectively. The PLGLAG peptide is a well-characterized substrate of MMP-2 and MMP-9, which are highly enriched in the tumor microenvironment.^[15] Melittin-containing polypeptides were expressed and purified (Figure 3a). Similar to the TN-APNPs, we found that only three polypeptides in combination, but not individual ones, formed nanoparticles (Figure 3b). The resulting melittin-loaded APNPs, designated as Mel-APNPs, were spherical in morphology and 5.8 nm in diameter (Figure 3c). CD spectroscopy confirmed that the formation of Mel-APNPs was driven by the formation of helical secondary structure (Figure

3d). Due to the inclusion of PLGLAG, Mel-APNPs were responsive to MMP-2 treatment and subsequently disassembled (Figure 3e).

Mel-APNPs exhibited limited toxicity in human breast cancer MDA-MB-231 cells and human glioma U87MG cells. However, upon treatment with MMP-2, Mel-APNPs killed tumor cells as efficiently as free melittin (Figure 3f; Figure S5a, Supporting Information). The antitumor effect of MMP-2-treated Mel-APNPs was due to the release of free melittin, since MMP-2 was deactivated by heating at 95 °C for 5 min after treatment. Melittin in the sequence released from Mel-APNPs had toxicity comparable to melittin in its native form (Figure S5b, Supporting Information). We tested Mel-APNPs for cancer treatment in mice bearing MDA-MB-231 tumors. Treatments were performed through intravenous injection of Mel-APNPs at 24 µg per mouse three times a week for two weeks. As shown in Figure 3g, we found that intravenous administration of Mel-APNPs efficiently inhibited tumor progression. By the end of the study, the average tumor size in the treatment group was 27% of that in the control group. Mice in both the control group and the treatment group did not show weight loss, suggesting that Mel-APNPs had limited toxicity for intravenous use (Figure S5c, Supporting Information). Terminal deoxynucleotidyl transferase (TdT) dUTP nick-end labeling (TUNEL) staining revealed massive cell apoptosis in tumors from mice that received Mel-APNP treatment (Figure S5d, Supporting Information).

Finally, we evaluated whether APNPs could be designed for targeted delivery of therapeutic peptides. For this purpose, we replaced the N-terminal “self” peptide in each polypeptide with RTIGPSV (Figure 4a). RTIGPSV is an iron-mimic peptide targeting the transferrin receptor (TfR) through binding with transferrin.^[16] TfR is highly expressed in tumor cells and has been extensively exploited for targeted delivery to tumors.^[17] Incorporation of RTIGPSV did not change the production of polypeptides nor the formation of nanoparticles (Figure S6a–d, Supporting Information). Resulting melittin-loaded TfR-APNPs, designated as TfR-Mel-APNPs, had size and morphology comparable to nontargeted APNPs, and were responsive to MMP-2 treatment (Figure S6e, Supporting Information). As expected, elimination of one “self” peptide decreased the circulation time within the blood (Figure S2e, Supporting Information). However, inclusion of the targeting peptide significantly enhanced the accumulation of APNPs in tumors. Targeted and nontargeted APNPs were labeled with AF750 and administered into tumor-bearing mice through tail vein injection. 24 h later, tumors were excised and imaged. We found that the concentration of targeted APNPs in tumors was 2.8 times greater than that of nontargeted APNPs (Figure 4b; Figure S6f, Supporting Information). Targeted delivery is capable of enhancing the antitumor effect of Mel.^[18] It is likely that treatment with TfR-Mel-APNPs will further augment the efficacy of Mel-APNPs shown in Figure 3g.

Compared to other delivery approaches, APNPs has several advantages. First, APNPs make it possible to deliver therapeutic peptides to targeted tissues without induction of systemic toxicity or side effects, and therefore have the potential to serve as a versatile platform for delivery of therapeutic peptides regardless of their toxicity or biological properties. In this study, we have demonstrated that APNPs can be employed to deliver a cell penetrant peptide, Tat-NR2B9c (type II), and a cytolytic peptide, melittin (type III). Because cargo peptides are embedded in APNPs and flanked by other fragments, they exhibit activities

only in the presence of enzymes that are highly enriched in the disease microenvironment. Second, APNPs are structurally simple but intrinsically multifunctional. APNPs are made of three polypeptides consisting of functional peptides as modular elements. In addition to the motifs providing therapeutic activities, APNPs include the “self” peptide for enhanced blood circulation. Further inclusion of additional functional modular sequence, such as a peptide for disease targeting, can be achieved. Third, APNPs are cost-effective for production and convenient for storage and delivery. Fabrication of APNPs simply requires production of proteins using *E. coli* or mammalian cells. Compared to traditional peptide synthesis, this approach has significantly reduced costs for production. The resulting APNPs are stable at room temperature and can be stored at low temperature for up to two months (Figure S7, Supporting Information), making it convenient for storage and delivery for clinical use.

In conclusion, we successfully used a complementary mechanism that is often used for guided synthesis of DNA or RNA nanoparticles for de novo design of APNPs. We demonstrated that APNPs allowed for efficient delivery of Tat-NR2B9c and melittin for disease treatment, and could be further engineered for targeted drug delivery. Due to their great capacity to accommodate therapeutic peptides without selectivity, their great safety profile regardless of the toxicity profile of cargo peptides, their intrinsically multifunctionality and simplicity, and their favorable cost-effectiveness for production and storage, we anticipate that APNPs will serve as a versatile platform for future clinical translation of therapeutic peptides.

Experimental Section

Polypeptide Gene Cloning, Expression, and Purification

Polypeptides were designed as shown in Figure 1. DNA codons for polypeptide were optimized for expression in *E. coli*, synthesized through Integrated DNA Technologies, Inc. (IDT), and cloned into a pTrcHis protein expression vector (Thermo Fisher Scientific). The sequences of polypeptides used in this study are included in Table S1 in the Supporting Information. Expression of polypeptides was carried out according to instructions described in the pTrcHis User Manual (Thermo Fisher Scientific). For purification of polypeptides for TN-APNP synthesis, pellets collected from 1 L culture of transformed *E. coli* were resuspended in 50 mL PBS with protease inhibitors [1×10^{-3} M phenylmethylsulfonyl fluoride (PMSF)], and sonicated in ice for 15 min (5 s burst, 3 s pause). After centrifugation at 18 000 rpm for 20 min at 4 °C, the supernatant was collected. The polypeptides in supernatant were purified using His60 Ni Superflow Resin & Gravity Columns according to the User Manual (Clontech). Polypeptides for synthesis of Mel-APNPs were purified from the inclusion bodies. Pellets collected from 1 L culture of transformed *E. coli* were resuspended, sonicated, and centrifuged according to the same procedures described above. After centrifugation, the pellets were used for purification. The pellets were washed sequentially with buffer A, which contained 50×10^{-3} M HEPES, 100×10^{-3} M NaCl, and 0.1 mg mL^{-1} lysozyme, and buffer B, which contained 1 M urea and 2% Triton X. To denature the inclusion bodies, the pellets were resuspended in 10 mL of 6 M Guanidinium chloride (GuaHCl), 100×10^{-3} M Tris 8.5, and 4×10^{-3} M PMSF. After 40 min, 1 mL of 200×10^{-3} M dithiothreitol (DTT) and 50 μL β -mercaptoethanol were added and incubated for 30 min. Then the

solution was diluted to 100 mL with solution containing 50×10^{-3} M Tris 10.7 and 4×10^{-3} M PMSF. After incubation at 4 °C for overnight, the solution was spun at 8000 rpm for 10 min to remove insoluble components. Denatured proteins in supernatant were renatured through gradient dialysis in GuaHCl solution with 50×10^{-3} M Tris 7.5 at a series of concentrations (0.3, 0.15, 0.1, and 0 M). After the last dialysis, the supernatant was collected and concentrated using MWCO 100,000 Ultrafilters (Millipore). Polypeptides in the supernatant were purified using His60 Ni Resin according to the User Manual.

Preparation of APNPs

To prepare APNPs, PP1, PP2, and PP3 were mixed at equal mole in PBS in the presence of tris(2-carboxyethyl) phosphine (TCEP) and Mal-PEG2000-NH₂ (JenKem Technology). In a typical reaction for synthesis of TN-APNPs, 0.6 mg of PP1 (MW 36 kDa, 0.254 mg mL⁻¹ in PBS 7.4), 0.5 mg of PP2 (MW 30 kDa, 0.233 mg mL⁻¹ in PBS 7.4), and 0.5 mg of PP3 (MW 30 kDa, 0.153 mg mL⁻¹ in PBS 7.4) were mixed in 10 mL PBS containing 0.7 mg TCEP (50 mol excess) and 5 mg Mal-PEG2000-NH₂ (2000 Da, 50 mol excess). After reacting at room temperature for 1 h, 20 mL of 8 M GuaHCl was added to make a final protein concentration of 0.05 mg mL⁻¹. After 1 h, the reactant was renatured through stepwise dialysis against GuaHCl solution at a series of concentrations (3, 2, 1.5, 1, 0.5, 0.25, and 0 M). To remove His tags, APNPs in supernatant were treated with recombinant enterokinase (rEK) according to the User Manual (EMD Millipore). The resulting APNPs were washed and concentrated using MWCO 100,000 Ultrafilters (Millipore), spun at 5000 rpm for 3 min to remove debris, filtered through a 0.22 μm membrane filter (Millipore), and stored at 4 °C. Concentrations of APNPs were determined by the standard BCA assay (Thermo Fisher Scientific). To prepare APNPs for TEM and AFM, PBS in APNP suspension was removed by washing with HPLC-grade water for three times using MWCO 100,000 Ultrafilters.

Supplementary Material

Refer to Web version on PubMed Central for supplementary material.

Acknowledgments

X.Y., X.G., P.W., L.H., and D.T. contributed equally to this work. This work was supported by NIH Grants NS095817 (J.Z.) and NS095147 (J.Z.), AHA grant 15GRNT25290018 (J.Z.), State of Connecticut, and NSFC grants 21233003 (L.F.), 21573019 (L.F.), 81271290 (X.G.), and 81471415 (X.G.). X.G. was partially supported by the Leading Disciplines Development Government Foundation of Shaanxi. MALS measurements were performed at the Yale University Facility for Light Scattering (FLS). ITC characterization was performed at the Biophysics Resource at Keck Facility at Yale School of Medicine.

References

1. Albericio F, Kruger HG. *Future Med. Chem.* 2012; 4:1527. [PubMed: 22917241]
2. Uhlig T, Kyprianou T, Martinellia TG, Oppicia CA, Heiligersa D, Hillsa D, Calvoa R, Verhaert P. *EuPA Open Proteomics.* 2014; 4:58.
3. a) GrandPre T, Li S, Strittmatter SM. *Nature.* 2002; 417:547. [PubMed: 12037567] b) Han L, Cai Q, Tian D, Kong DK, Gou X, Chen Z, Strittmatter SM, Wang Z, Sheth KN, Zhou J. *Nanomedicine.* 2016; 12:1833. [PubMed: 27039220]

4. Aarts M, Liu Y, Liu L, Besshoh S, Arundine M, Gurd JW, Wang YT, Salter MW, Tymianski M. *Science*. 2002; 298:846. [PubMed: 12399596]
5. Hill MD, Martin RH, Mikulis D, Wong JH, Silver FL, Terbrugge KG, Milot G, Clark WM, Macdonald RL, Kelly ME, Boulton M, Fleetwood I, McDougall C, Gunnarsson T, Chow M, Lum C, Dodd R, Poublanc J, Krings T, Demchuk AM, Goyal M, Anderson R, Bishop J, Garman D, Tymianski M. ENACT Trial Investigators. *Lancet Neurol*. 2012; 11:942. [PubMed: 23051991]
6. Gajski G, Garaj-Vrhovac V. *Environ. Toxicol. Pharmacol*. 2013; 36:697. [PubMed: 23892471]
7. Papadopoulou LC, Tsiftoglou AS. *Pharmaceuticals*. 2013; 6:32. [PubMed: 24275786]
8. a) Campolongo MJ, Tan SJ, Xu JF, Luo D. *Adv. Drug Deliv. Rev*. 2010; 62:606. [PubMed: 20338202] b) Shu D, Shu Y, Haque F, Abdelmawla S, Guo PX. *Nat. Nanotechnol*. 2011; 6:658. [PubMed: 21909084]
9. Rodriguez PL, Harada T, Christian DA, Pantano DA, Tsai RK, Discher DE. *Science*. 2013; 339:971. [PubMed: 23430657]
10. a) Reinke AW, Grant RA, Keating AE. *J. Am. Chem. Soc*. 2010; 132:6025. [PubMed: 20387835] b) Gradisar H, Bozic S, Doles T, Vengust D, Hafner-Bratkovic I, Mertelj A, Webb B, Sali A, Klavzar S, Jerala R. *Nat. Chem. Biol*. 2013; 9:362. [PubMed: 23624438]
11. Zhou L, Li F, Xu HB, Luo CX, Wu HY, Zhu MM, Lu W, Ji X, Zhou QG, Zhu DY. *Nat. Med*. 2010; 16:1439. [PubMed: 21102461]
12. Cook DJ, Teves L, Tymianski M. *Sci. Transl. Med*. 2012; 4:154ra133.
13. Whitney M, Savariar EN, Friedman B, Levin RA, Crisp JL, Glasgow HL, Lefkowitz R, Adams SR, Steinbach P, Nashi N, Nguyen QT, Tsien RY. *Angew. Chem., Int. Ed*. 2013; 52:325.
14. DeGrado WF, Musso GF, Lieber M, Kaiser ET, Kezdy FJ. *Biophys. J*. 1982; 37:329. [PubMed: 7055625]
15. Jiang T, Olson ES, Nguyen QT, Roy M, Jennings PA, Tsien RY. *Proc. Natl. Acad. Sci. USA*. 2004; 101:17867. [PubMed: 15601762]
16. Staquicini FI, Ozawa MG, Moya CA, Driessen WH, Barbu EM, Nishimori H, Soghomonyan S, Flores LG 2nd, Liang X, Paolillo V, Alauddin MM, Basilion JP, Furnari FB, Bogler O, Lang FF, Aldape KD, Fuller GN, Hook M, Gelovani JG, Sidman RL, Cavenee WK, Pasqualini R, Arap W. *J. Clin. Invest*. 2011; 121:161. [PubMed: 21183793]
17. a) Kawamoto M, Horibe T, Kohno M, Kawakami K. *BMC Cancer*. 2011; 11:359. [PubMed: 21849092] b) Dufes C, Al Robaian M, Somani S. *Ther. Deliv*. 2013; 4:629. [PubMed: 23647279]
18. Soman NR, Baldwin SL, Hu G, Marsh JN, Lanza GM, Heuser JE, Arbeit JM, Wickline SA, Schlesinger PH. *J. Clin. Invest*. 2009; 119:2830. [PubMed: 19726870]

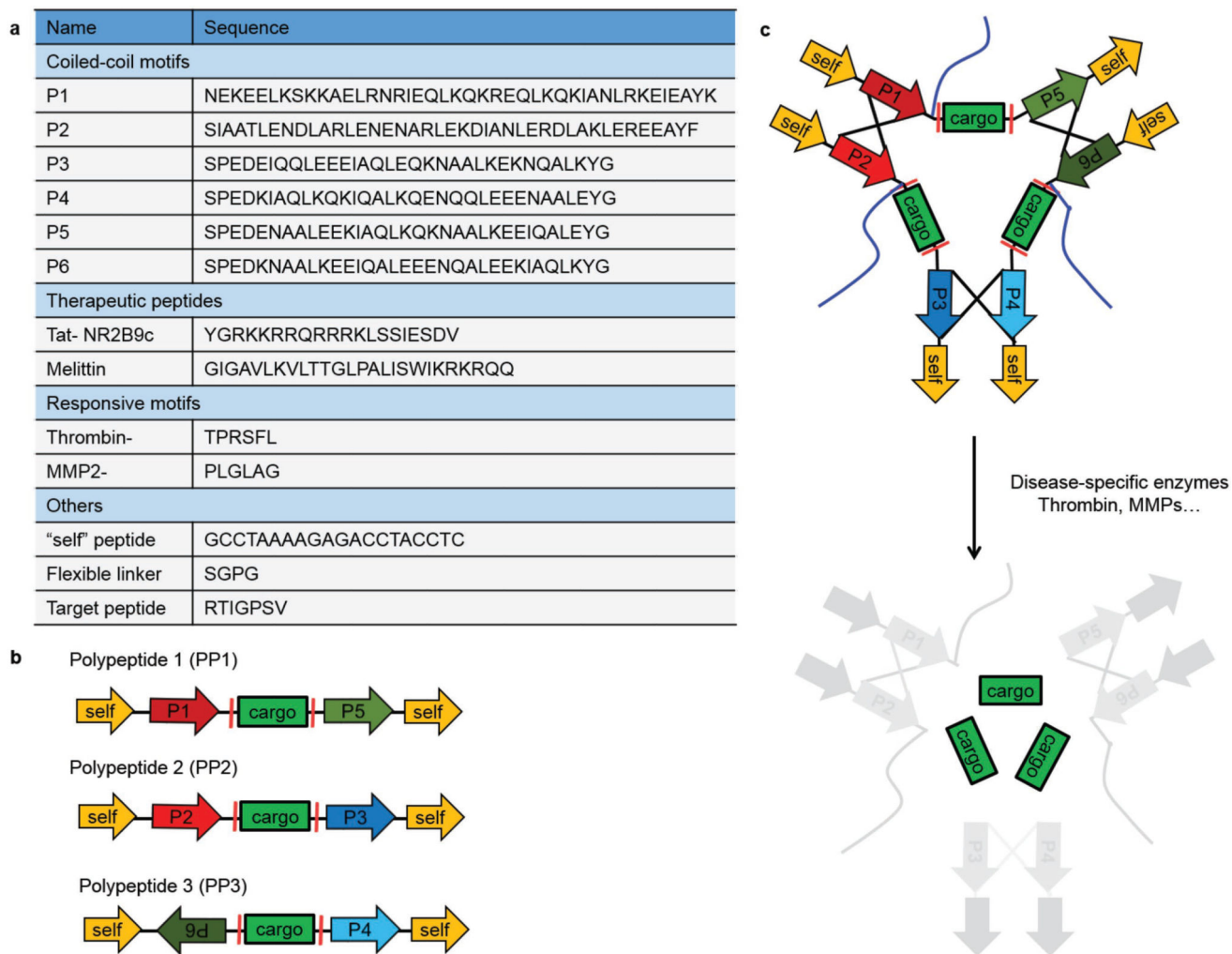


Figure 1. Design of APNPs. a) Function and sequences of modular peptides used in the study. b) Schematic of polypeptides containing functional modular motifs. c) Formation and activation of APNPs. APNPs are self-assembled through pairwise coiled-coil dimerization and activated by proteases in disease microenvironment. Blue lines represent PEG molecules.

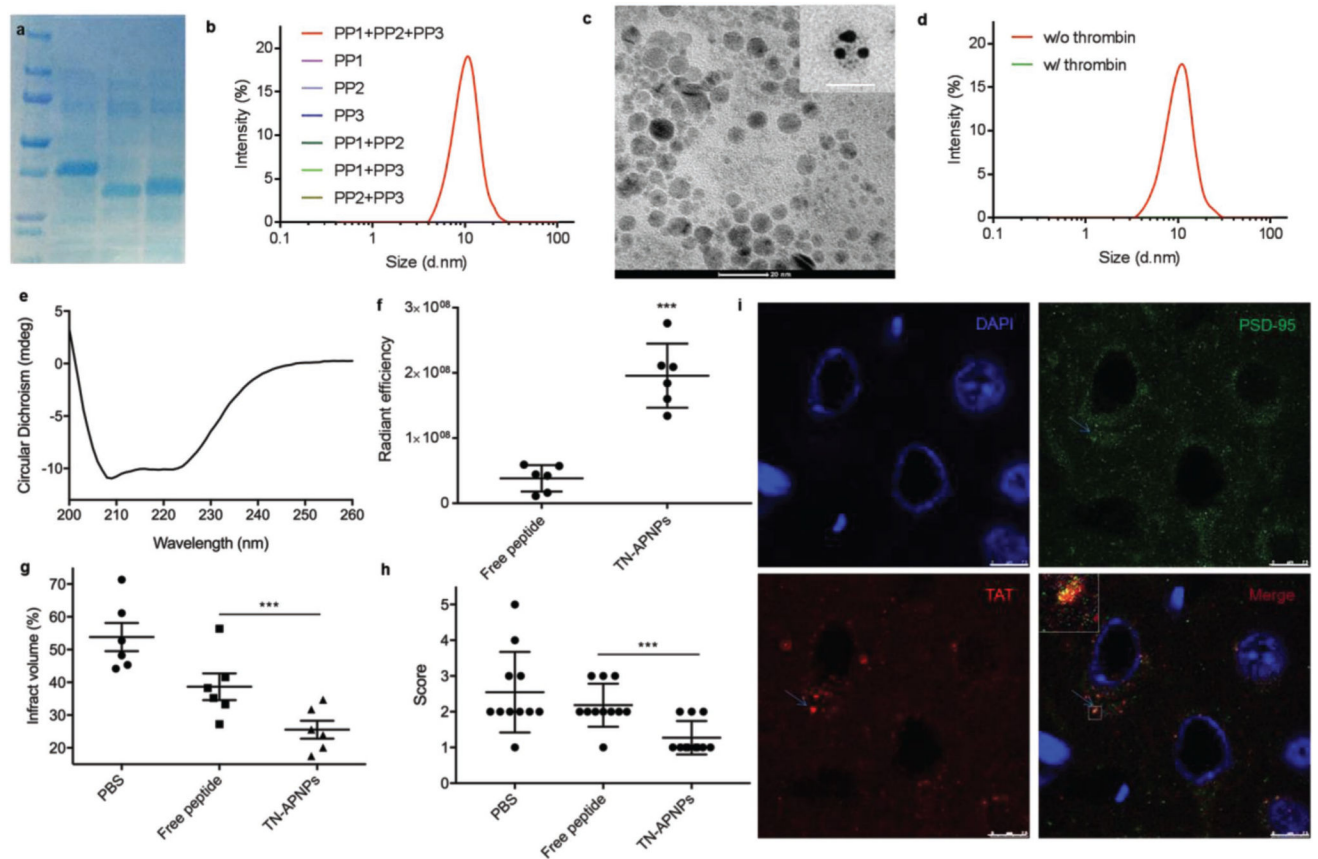


Figure 2.

Formulation, characterization, and evaluation of TN-APNPs. a) Expression and purification of polypeptides. b) DLS analysis revealed that only three polypeptides, but not individual ones, form APNPs. c) A representative TEM image of TN-APNPs and close-up views of individual APNPs stained with 5 nm Ni-NTA–nanogold beads (insert) Scale bar: 20 nm. d) DLS analysis of the secondary structure of TN-APNPs. e) TN-APNPs were disassembled after thrombin treatment. f) In vivo quantitative distribution of Tat-NR2B9c in the ischemic region after delivery in form of free peptide or APNPs. Both free Tat-NR2B9c and TN-APNPs were labeled with AF750. Each MCAO rat received the same amount of AF750 immediately after surgery. 24 h later, rats were euthanized. The brains were harvested and subjected to IVIS imaging. Fluorescence intensity in the ischemic region was determined using Living Image 3.0. Fluorescence unit determined by IVIS was expressed as radiance efficiency [$(\text{photons s}^{-1} \text{cm}^{-2} \text{sr}^{-1})/(\mu\text{W cm}^{-2})$]. g) Infarct volumes in rats received indicated treatments. The ischemic region was identified by TTC staining and quantified by ImageJ (NIH). h) Neurological scores of MCAO rats receiving indicated treatments at day 3 after surgery. i) Confocal analysis of the interaction of PSD-95 and Tat-NR2B9c in a representative ischemic region. PSD-95 and Tat-NR2B9c were identified by an anti-PSD-95 antibody and an anti-TAT antibody, respectively. Scale bar: 7.5 μm .

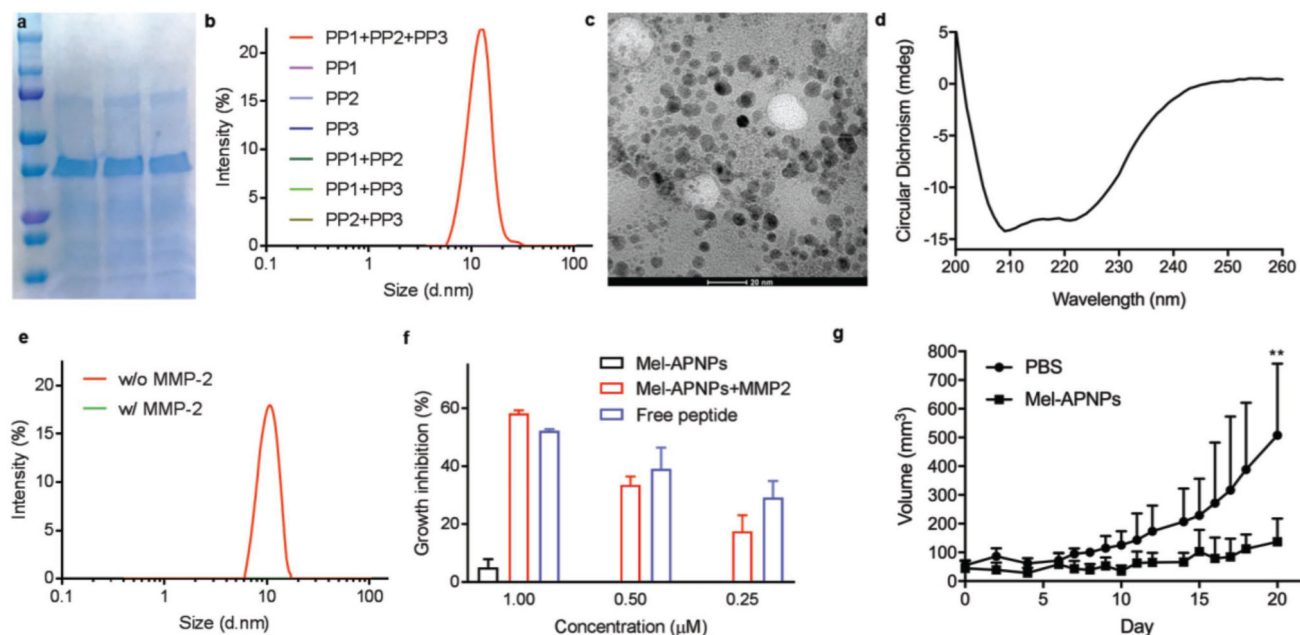


Figure 3. Formulation, characterization, and evaluation of Mel-APNPs. a) Expression and purification of polypeptides. b) DLS analysis revealed that only three polypeptides, but not individual ones, form Mel-APNPs. c) A representative TEM image of Mel-APNPs (scale bar: 20 nm). d) CD analysis of the secondary structure of Mel-APNPs. e) Mel-APNPs were disassembled after MMP-2 treatment. f) Cytotoxicity of Mel-APNPs with and without MMP-2 treatment and free melittin peptide on MDA-MB-231 cells. Mel-APNPs without MMP-2 treatment exhibited limited toxicity. Mel-APNPs after MMP-2 treatment showed cytotoxicity similar to free melittin. g) Antitumor effect of Mel-APNPs evaluated in mice bearing MDA-MB-231 tumors. Tumor-bearing mice were treated three times a week with intravenous injection of PBS or Mel-APNPs ($n = 7$ mice per group).

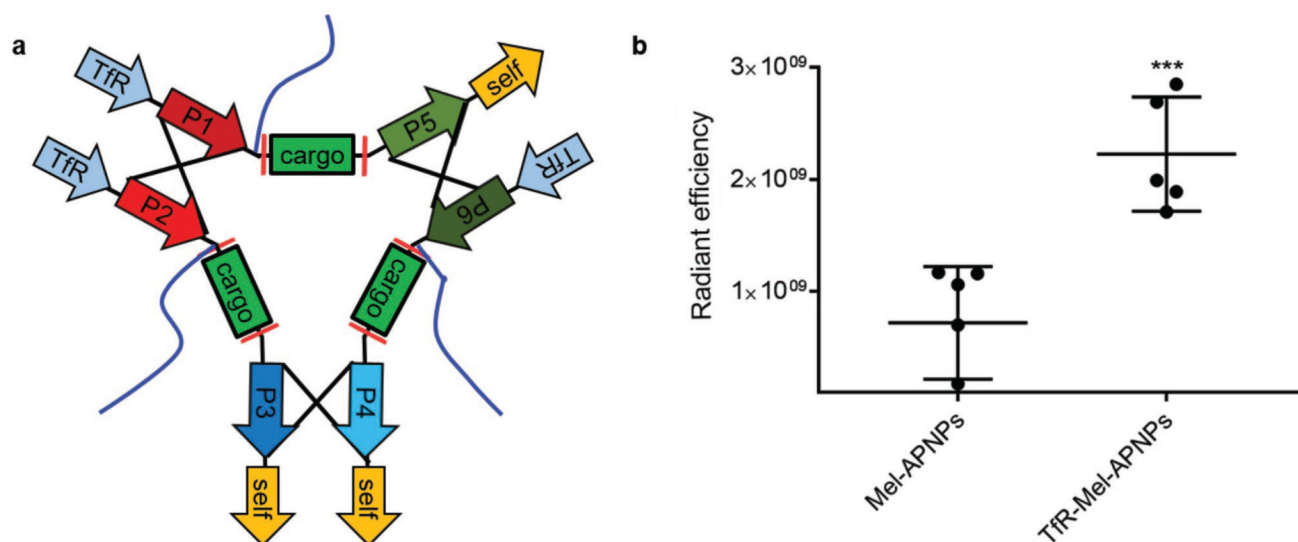


Figure 4. Tfr-Mel-APNPs for targeted delivery to tumors. a) Schematic of Tfr-Mel-APNPs. b) In vivo quantitative distribution of Mel-APNPs with and without target ligand RTIGPSV. When tumor volume reached $\approx 200 \text{ mm}^3$, mice were grouped and received treatment of AF750-labeled APNPs. 24 h later, mice were euthanized. The tumors were harvested and subjected to IVIS imaging. Fluorescence intensity in the ischemic region was determined using Living Image 3.0.